Inorganic Chemistry

Article

pubs.acs.org/IC

Two-Dimensional Bicapped Supramolecular Hybrid Semiconductor Material Constructed from the Insulators α-Keggin Polyoxomolybdate and 4,4′-Bipyridine

Abishek K. Iyer and Sebastian C. Peter*

New Chemistry Unit, Jawaharlal Nehru Centre for Advanced Scientific Research, Jakkur, Bangalore, 560064 India

Supporting Information

ABSTRACT: A new organic−inorganic hybrid material $[SiMo_{14}O_{44}](H4,4'\text{-bpy})_2\cdot xH_2O$ (4,4′-bpy = 4,4′-bipyridine) was synthesized using a hydrothermal method. The compound was characterized using single crystal X-ray diffraction (XRD), infrared spectroscopy (IR), ultraviolet−visible spectroscopy (UV−vis), and X-ray photoelectron spectroscopy (XPS). XRD studies on selected single crystals suggested that the compound consists of supramolecular 2D layer structures composed of capped α-Keggin polyoxomolybdate anions and 4,4′-bpy organic ligands. Absorption measurements show a band gap of 2.99 eV in the hybrid which suggests a semiconducting nature compared to the insulating free α-Keggin and 4,4′-bpy. The magnetic susceptibility of the hybrid material was investigated in the temperature range 1.8−300 K obeying the Curie−Weiss law above 70 K. Experimentally measured magnetic moment of 2.71 μ_B/formula indicates possible mixed valent molybdenum in the compound. The XPS measurements confirm the presence of both Mo^V and Mo^{VI} in the ratio 15:85 resulting in the structural formula of the hybrid as $[SiMo^V_2Mo^{VI}_{12}O_{44}](H4,4'\text{-bpy})_2\cdot xH_2O$.

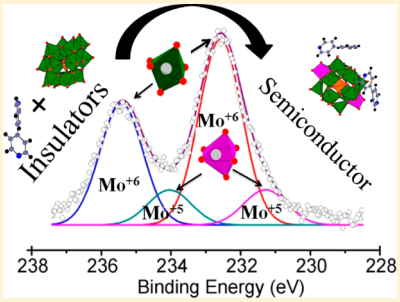

1. INTRODUCTION

During the last two decades, the design and synthesis of directed supramolecular arrays assembled with metal oxides to give organic−inorganic hybrid materials have received considerable attention due to their potential applications in molecular electronics, sensor design, magnetism, biochemistry, catalysis, and photochemistry.[1−13] Recently, polyoxometalate (POM) anion clusters were used as the building units for the construction of extended high-dimensional organic−inorganic hybrid materials with novel structures and unusual properties.[14−23] The selection of organic fragments for the construction of hybrid materials is a key factor, as they are expected to act as charge compensating, space-filling, or structure-directing agents and even may adopt a variety of substructural patterns from zero- to one-dimensional (1D),[24,25] two-dimensional (2D),[26] and/or three-dimensional (3D) arrays.[27]

The interactions in these organic−inorganic hybrids have been reported previously[28−35] and can be divided into two types. The first type contains the assembly of the inorganic and organic moieties through π···π stacking, electrostatic, hydrogen bonding, and/or van der Waals interactions.[34] While in the second type, the covalent interactions can exist between the inorganic and organic parts.[35] The H-bonding along with electrostatic interactions in the first type play a unique role in controlling directionality and strength over a short range in these hybrids.[33]

POMs are nanosized metal oxide clusters which can act as receptors to form hydrogen bonding with other organic/inorganic moieties due to many surface oxygen atoms. The ligand 4,4′-bipyridine (4,4′-bpy) is an interesting candidate for linking with cluster metal atoms in the growth of coordination networks due to the following features: it has two potential binding sites which are arranged in a divergent (*exo*) fashion having a rigid structure which will help in the predictability of the network geometries; the length of the ligand is good enough to create the cavities of molecular dimensions upon the formation of the networks with cluster atoms. In principle, the pyridyl groups of 4,4′-bpy can rotate along a central C−C bond. However, the rotation does not affect the mutual orientation of the two lone pairs. Therefore, 4,4′-bpy can be regarded as a rigid and prototypical bridging ligand,[36] and is often used as a pillaring agent in the construction of hybrids based on a metal−organic framework.[37−41] 4,4′-bpy is a monodentate ligand which increases the probability of the interaction with the POM either covalently or through other interactions. Though there are several hybrid materials based on POMs and metal coordination complexes reported, only a few materials containing direct interactions between POMs and 4,4′-bpy were found. Those are $[(HSiMo_{12}O_{40})(H4,4'\text{-bpy})_2]\text{-}[(H4,4'\text{-bpy})(H_2O)_2]\cdot 2H_2O$,[42] $[(HSiW_{12}O_{40})(H4,4'\text{-bpy})_2]\text{-}[(H4,4'\text{-bpy})(H_2O)_2]\cdot 2H_2O$,[42] $[(SiW_{12}O_{40})(H4,4'\text{-bpy})_4]\text{-}(4,4'\text{-bpy})\cdot 2H_2O$,[42] $(H_24,4'\text{-bpy})(H4,4'\text{-bpy})_2[SiW_{12}O_{40}]\cdot 4H_2O$, $(H_24,4'\text{-bpy})(H4,4'\text{-bpy})[PMo_{12}O_{40}]$,[43] $[H4,4'\text{-bpy}]_2[HPW_{12}O_{40}]\cdot H_2O$,[44] $[H_24,4'\text{-bpy}]_6[P_2W_{18}O_{62}]_2\cdot 6H_2O$,[44] $[H_24,4'\text{-bpy}]_5[HP_2W_{18}O_{62}]_2$,[44] and $(H_24,4'\text{-bipy})_2[SiW_{12}O_{40}]\cdot(4,4'\text{-bipy})\cdot 6H_2O$.[45]

Received: November 16, 2013
Published: December 23, 2013

   dx.doi.org/10.1021/ic402858u | *Inorg. Chem.* 2014, 53, 653−660

In this Article, we report the synthesis and characterization of a new compound having a directly linked POM with 4,4′-bpy ligand: $[(4,4'\text{-Hbpy})_2(SiMo_{14}O_{44})]$ ($SiMo_{14}$-bpy_2). The crystal structure of $SiMo_{14}$-bpy_2 was studied using the X-ray diffraction data obtained from the single crystal. In $SiMo_{14}$-bpy_2, 4,4′-bpy serves as a bridging unit to activate the transition metal for the formation of highly dimensional frameworks. Though there are several hybrid compounds constructed from POM and 4,4′-bpy based metal complexes, there has been no report for the direct linkage between $(SiMo_{14}O_{44})^{6-}$ and any organic ligand other than tetramethylammonium hydroxide (TMA)[46] and $[Fe(C_8H_7N_3)_3]$.[47] The $SiMo_{14}$-bpy_2 is the first supramolecular polyoxometalate-organic hybrid containing a bicapped α-Keggin structure with 4,4′-bpy. We have compared the crystal structure of $SiMo_{14}$-bpy_2 with its parent compound $[(H4,4'\text{-bpy})_3(SiMo_{12}O_{40})]$ ($SiMo_{12}$-bpy_3). Absorption studies within the UV−vis range suggest the new hybrid material is a semiconductor with a band gap of 2.99 eV. IR spectroscopy, SEM/EDAX analysis, and XPS of both compounds have been compared and discussed in detail. We also performed preliminary magnetic measurements of the compound $SiMo_{14}$-bpy_2. XPS and magnetic measurements suggests the hybrid material contains molybdenum in a mixed valent state which was found to corroborate with crystal structure.

2. EXPERIMENTAL SECTION

2.1. Synthesis. $Na_2MoO_4{\cdot}2H_2O$ and Na_2SiO_3 were purchased from Sigma-Aldrich, and $CuCl_2{\cdot}2H_2O$ was purchased from Alfa Aesar. Concentrated HCl was purchased from Thomas Bekar. The hydrothermal synthesis was carried out in a 23 mL Teflon lined stainless steel containers under autogenous pressure. The reaction vessel was filled to approximately 75% volume capacity (V_i = 18 mL). $Na_2MoO_4{\cdot}2H_2O$ (0.5 g, 2.07 mmol) was added to the acetate buffer of pH 4 in the autoclave. Na_2SiO_3 (0.5 g, 1.759 mmol) and $CuCl_2{\cdot}2H_2O$ (333 mg, 1.36 mmol) were added immediately followed by the addition of 4,4′-bpy. A 1 mL portion of concentrated HCl (11.3 N) was added to the turbid solution to make the pH of the solution close to 2. $Na_2MoO_4{\cdot}2H_2O$, Na_2SiO_3, conc HCl (11.3 N), 4,4′-bpy, and H_2O were taken in the molar ratio 1:2:100:n:5000, with n as a variable parameter ($10 < n < 30$) to adjust the initial pH. The final pH of the solution was made to 1.6 by addition of concentrated HCl. The reaction was kept at 160 °C for 5 days. The autoclave was cooled down to room temperature within 12 h. The products were decanted and washed with ethanol. Dark blue tetragonal biprismatic shaped crystals $SiMo_{14}$-bpy_2 along with block shaped crystals $SiMo_{12}$-bpy_3 were obtained approximately in 61% and 19% yield, respectively, based on the initial $Na_2MoO_4{\cdot}2H_2O$.

2.2. Powder X-ray Diffraction (XRD). Phase identity and purity of the compounds were determined by powder XRD experiments that were carried out with a Bruker X8 Discover diffractometer using Cu Kα radiation (λ = 1.541 87 Å). The data was collected over the angular range $5° \le 2\theta \le 90°$, with a step size of 0.07° at room temperature calibrated against corundum standards. The powder XRD comparison with the simulated single crystal XRD pattern is shown in the Supporting Information (Figure S1).

2.3. Single Crystal XRD. A suitable single crystal of the compound $SiMo_{14}$-bpy_2 was mounted on a thin glass fiber with commercially available super glue. X-ray single crystal structural data of the samples were collected on a Bruker X8 APEX II diffractometer equipped with a normal focus, 2.4 kW sealed tube X-ray source with graphite monochromatic Mo Kα radiation (λ = 0.710 73 Å) operating at 50 kV and 30 mA, with ω scan mode. The program SAINT[48] was used for integration of diffraction profiles, and absorption corrections were made with SADABS program.[49] All the structures were solved by direct method and followed by successive Fourier and difference Fourier syntheses. All the non-hydrogen atoms were refined anisotropically. Calculations were carried out using SHELXL 97, SHELXS 97, PLATON, and WinGX system, ver 1.80.05.[50,51] The crystallographic details are in Table 1.

Table 1. Crystal Data and Structure Refinement for $[SiMo_{14}O_{44}](H4,4'\text{-bpy})_2$ at 293(2) K

empirical formula	$C_{20}H_{16}N_4SiMo_{14}O_{44}$
fw	2387.62
T	296(2)K
wavelength	0.71073 Å
cryst syst	monoclinic
space group	$P2_1/n$
unit cell dimensions	a =13.7874(3) Å, α = 90.00°
	b = 18.6536(4) Å, β = 105.27°(2)
	c = 19.5220(4) Å, γ = 90.00°
V	4843.48 (14) Å^3
Z	4
density (calcd)	3.27 g/cm^3
abs coeff	3.639 mm^{-1}
F(000)	4469
crystal size	0.5 × 1 × 0.1 mm^3
θ range for data collection	1.5−29.0°
index ranges	$-18 \le h \le 18$
	$-23 \le k \le 25$,
	$-26 \le l \le 24$
reflns collected	109 920
indep reflns	12 880 [R_{int} = 0.0495]
completeness to θ = 30.55°	100%
refinement method	full-matrix least-squares on F^2
data/restraints/params	12 880/0/749
GOF	1.240
final R indices[a] [$>2\sigma(I)$]	R_{obs} = 0.047, wR_{obs} = 0.133
extinction coeff	0.0017
largest diff peak and hole	2.231 and −2.822 e Å^{-3}

[a] $R = \Sigma||F_o| - |F_c||/\Sigma|F_o|$, $wR = \{\Sigma[w(|F_o|^2 - |F_c|^2)^2]/\Sigma[w(|F_o|^4)]\}^{1/2}$, and calcd $w = 1/[\sigma^2(F_o^2) + (0.0318P)^2 + 111.1197P]$ where $P = (F_o^2+2F_c^2)/3$.

2.4. Fourier Transform Infrared Spectroscopy. FT-IR spectra were obtained for powder samples of $SiMo_{12}$-bpy_3 and $SiMo_{14}$-bpy_2 on a Bruker IFS 66v/S. The pellets were prepared with KBr, and the KBr spectrum was used a reference.

2.5. UV−Vis and Luminescence Spectroscopy. Emission spectra within the UV−vis−NIR region for the samples 4,4′-bpy, $SiMo_{12}$-bpy_3, and $SiMo_{14}$-bpy_2 were recorded on Perkin-Elmer Ls 55 luminescence spectrometer. The samples were loaded in a $BaSO_4$ crucible, and the measurements were performed in the range 200−800 cm^{-1}. All obtained spectra were subtracted with $BaSO_4$ as the background. The solid state fluorescence studies were performed by loading the sample in a transparent holder, and the measurements were performed only on the samples.

2.6. Scanning Electron Microscopy (SEM)−Energy Dispersive X-ray Spectroscopy (EDAX). The samples were loaded on a carbon tape, and the measurement was done on the Leica 220i microscopy instrument and Bruker 129 eV EDAX instrument. The EDAX measurement were performed on single crystals with clean surface. From the EDAX of various collected crystals we confirmed the presence of all the elements in the spectrum as shown in the Supporting Information (Figure S2).

2.7. X-ray Photoelectron Spectroscopy. XPS spectra for the samples $SiMo_{12}$-bpy_3 and $SiMo_{14}$-bpy_2 were collected as a function of isochronal annealing (1 min) at increasingly high temperature up to 940 K (with XPS spectra being recorded on cooling to 300 K).

2.8. Magnetic Measurements. Magnetic measurements of the samples $SiMo_{12}$-bpy_3 and $SiMo_{14}$-bpy_2 were carried out on a Quantum Design MPMS-SQUID magnetometer. Measurements were per-

dx.doi.org/10.1021/ic402858u | Inorg. Chem. 2014, 53, 653−660

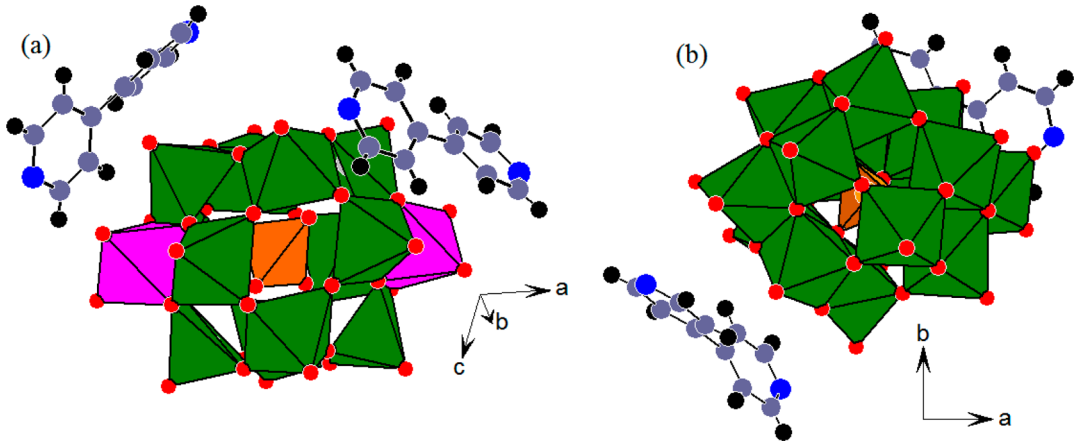

Figure 1. (a) Polyhedra representation of $[SiMo_{14}O_{44}](H4,4'\text{-bpy})_2$ where the pink polyhedral corresponds to the $\{MoO_2\}$ unit and (b) polyhedral representation of $[SiMo_{12}O_{40}](H_24,4'\text{-bpy})_2$. The green color polyhedral in both structures corresponds to the Mo coordination sphere while the orange color polyhedral corresponds to the Si tetrahedral coordination sphere.

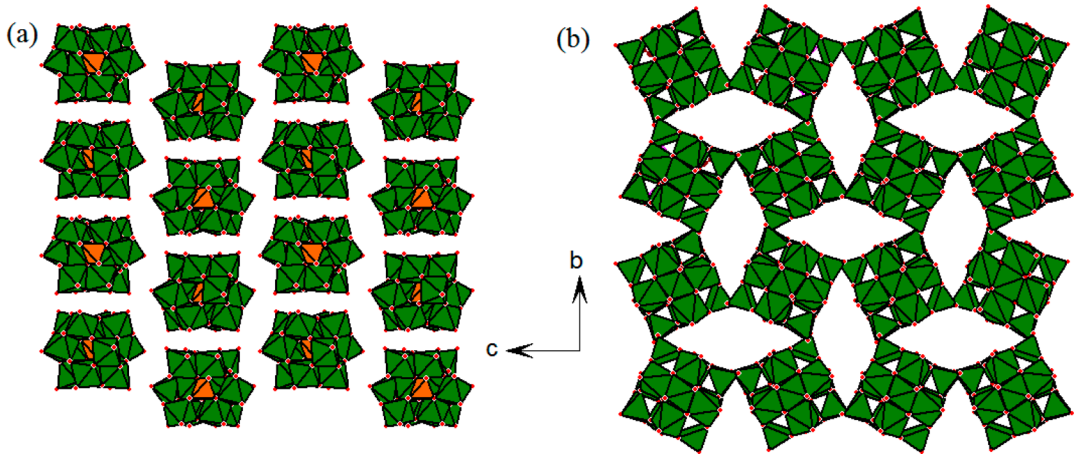

Figure 2. Orientation of (a) the polyoxometalate units $[SiMo_{12}O_{40}]$ in $SiMo_{12}$-bpy_3 and (b) $[SiMo_{14}O_{44}]$ in $SiMo_{14}$-bpy_2 along the *a*-axis. The 4,4′-bpy moieties are removed for the better representation.

formed on polycrystals, which were ground and screened by powder XRD to verify phase identity and purity. Temperature dependent magnetic susceptibility data were collected for field cooled mode (FC) between 2 to 300 K with an applied field of 1 kG.

3. RESULTS AND DISCUSSION

3.1. Synthesis and Characterization. The main aim of the work was to study the chemistry of inorganic organic hybrid materials made up of POMs with metal coordination complexes. During our systematic studies on the Cu based complexes, copper chloride was used as the source for Cu. However, the X-ray diffraction data on two different shapes of single crystals showed the formation of two products $SiMo_{14}$-bpy_2 and $SiMo_{12}$-bpy_3 having the direct linkage between POMs and 4,4′-bpy. Later, a similar synthesis strategy was attempted in the absence of $CuCl_2$ leading to the formation of only blue powder with no crystals.

The role of $CuCl_2$ in the formation of the single crystals is not clearly understood, and kinetic studies would be required to understand the exact role of the salt. However, one way to understand is by the ion strength of the solution as mentioned by Xu et al.[28] The ion strength could play a role in the synthesis, where the addition of the salt to the reaction mixture increases the ion strength of the solution 0.87 mmol/mL, but in the absence of $CuCl_2$ (1.36 mmol) the ionic strength is 0.51 mmol/mL. This could be one of the reasons for the formation of the sample $SiMo_{12}$-bpy_3, but the formation of the sample $SiMo_{14}$-bpy_2 could also be influenced by the initial pH and the final pH. Interestingly, we have observed the formation of the different compound which is beyond the scope of this Article. Possibly, the mechanism may be such that when the pH = 4, the formation of the α-Keggin is favored, but the sudden decrease in the pH results in the two units acting as protonating agents on the four terminal oxygen.[46] This $\{MoO_2\}$ unit is added to the center of inversion to give the most stable product.

The reaction when performed without $CuCl_2$ maintaining the initial pH at 4 resulted in no crystallization. Reaction when also performed in water (pH = 5.63) without using the buffer solution gave a poor yield of $SiMo_{14}$-bpy_2, but the more thermodynamically stable compound $SiMo_{12}$-bpy_3 was formed with a yield of 72% based on the initial concentration of $NaMoO_4{\cdot}2H_2O$. These controlled reactions suggest that pH has a significant role in the formation of these compounds. Both the compounds were found to be air stable and only partially soluble in *N*,*N*′-dimethyformamide (DMF). The dark blue color of the crystals suggests intervalence charge transfer transitions and is characteristic of "molybdenum blue" species[52] indicating the mixed-valent molybdenum (Mo^V and Mo^{VI})

dx.doi.org/10.1021/ic402858u | *Inorg. Chem.* 2014, 53, 653−660

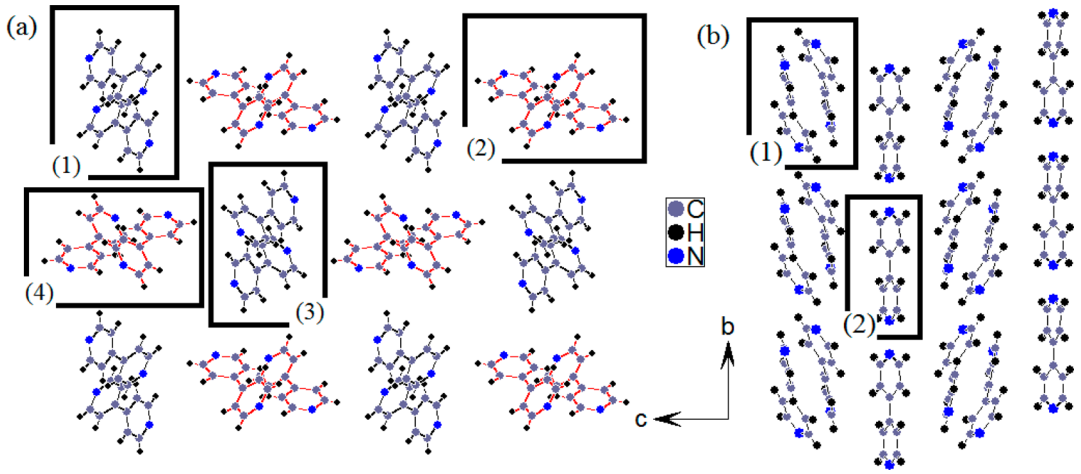

Figure 3. Orientation of the 4,4′-bpy ligands in the compounds (a) $SiMo_{12}$-bpy_3 and (b) $SiMo_{14}$-bpy_2. The solid black color boxes with numbers on the corner represent different types of orientation in the 4,4′-bpy rings.

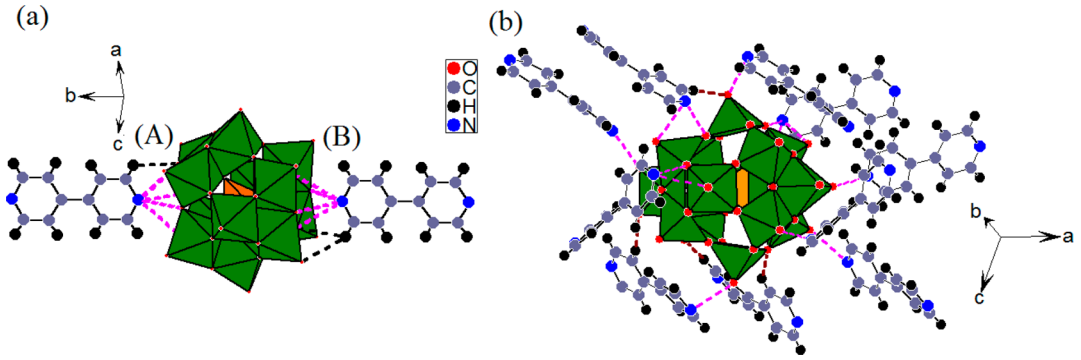

Figure 4. (a) Interaction of the 4,4′-bpy rings with the hybrid (a) $[SiMo_{12}O_{40}](H_2$4,4′-bpy$)_3$ and (b) $[SiMo_{14}O_{44}]$ (H4,4′-bpy$)_2$. The electrostatic bonds and hydrogen bonds are represented in pink and black, respectively.

atoms. The reduction of Mo^V to Mo^{VI} under hydrothermal conditions was due to the lower pH of the solution, which has been previously reported by Haushalter and Mundi.[53]

3.2. Crystal Structure. The asymmetric unit of $SiMo_{14}$-bpy_2 is made up of one $[SiMo_{14}O_{44}]^{4-}$ ($SiMo_{14}$) unit surrounded by two H4,4′-bpy molecules as shown in Figure 1a. There are 14 different Mo atomic sites occupying the Wyckoff site 4*e*. The crystal structure of $[SiMo_{14}O_{44}]$ has been previously explained by Dolbecq et al.[46] The structure consists of α-Keggin framework $[SiMo_{14}O_{44}]^{6-}$ ($SiMo_{14}$), which is a reduced form of the α-Keggin anion with two $\{MoO_2\}$ capped units along the center of inversion. At high temperature and low pH, α-Keggin unit is first reduced to give a hypothetical five-electron reduced α-Keggin structure with two $\{Mo^VO_2\}$ capping units. This reduced α-Keggin structure is stabilized by the 4,4′-bpy via hydrogen bonding and electrostatic interaction. The basic α-Keggin unit has a C_4 axis of rotation which is distorted due to two oppositely positioned $\{MoO_2\}$ units, which changes the central axis that seems to result in the tilt in the $SiMo_{14}$-bpy_2 framework. This tilted structure can be seen in Figure 2b. This tilt seems to play a significant role in the interaction of the 4,4′-bpy moieties with the POM structure (discussed below). There are three different types of metal oxygen bonds: 1.834−2.193 Å for Mo−O_b (O_b = bridging oxygen), 1.672−1.702 Å for Mo−O_t (O_t = terminal oxygen) of the MoO_6 unit, and 2.353−2.375 Å for Mo−O_c (O_c = central oxygen of Mo−O−Si). The variable bond lengths play a significant role in the distortion in the Mo octahedra. The distortion is the least for $Mo(13)O_6$ and $Mo(14)O_6$ octahedra (two $\{MoO_2\}$ capped units also form octahedral utilizing the oxygen of the other units) due to the presence of two free O atoms. The bond valence sum (BVS)[54] calculation was performed to understand the valence of Mo atoms, and it was found that an average value was 5.82 for 12 Mo atoms (Mo(1)−Mo(12)) indicating the oxidation state of these molybdenum atoms is +6 while BVS calculated for Mo(13) and Mo(14) atoms is 5.47 indicating that the Mo atoms in the $\{MoO_2\}$ subunits exist in the +5 oxidation state. This mixed valent nature is confirmed by magnetic measurements and quantitatively measured by XPS measurements and will be discussed in the later sections. On the basis of the crystal structure and XPS, the formula for the hybrid material can be represented as $[SiMo^{+V}{}_2Mo^{+VI}{}_{12}O_{44}](H4,4'\text{-bpy})_2$.

$SiMo_{14}$-bpy_2 crystallizes in the monoclinic space group $P2_1/n$ with lattice parameters a = 13.7874(3) Å, b = 18.6536(4) Å, c = 19.5220(4) Å, β = 105.27(2)°. In a comparison of this with the reported $(TMA)_4SiMo_{14}O_{44}$[46] having lattice parameters a = 12.0502(4) Å, b = 11.7500(4) Å, c = 19.8001(4) Å, β = 100.52(1)° and the same space group, a significant enhancement in the b-axis of $SiMo_{14}$-bpy_2 was observed. The other reported compound $[Fe(C_8H_7N_3)_3]_2[SiMo_{14}O_{44}]$ was also found in the monoclinic system, but with c-glide plane and lattice parameters a = 13.055(3) Å, b = 16.931(3) Å, c = 18.562(4) Å, β = 102.69(3)°, and also with a substantial increase in the b-axis. The enhancement in the lattice parameters can be explained on the basis of the different length of the organic parts in the

dx.doi.org/10.1021/ic402858u | *Inorg. Chem.* 2014, 53, 653−660

hybrid materials. The length of one $SiMo_{14}O_{44}$ unit is ~10.508(14) Å; however, the length of one molecule of TMA and 4,4′-bpy is ~1.18 and 6.9 Å, respectively. Along the *b*-axis of $(TMA)_4SiMo_{14}O_{44}$, one $SiMo_{14}O_{44}$ with a tilt angle of 62.34(3)° and two half TMA occupy with a unit cell length close to 11.75(4) Å.[32] In the new compound $SiMo_{14}$-bpy_2 the unit cell along the *b*-axis comprises two $SiMo_{14}O_{44}$ units tilted at an angle of 41.14(2)° (Figure 2b) with a unit length of 18.6536(4) Å. Due to this tilting, all 14 MoO_6 octahedra are distorted substantially with six different Mo−O bond distances. All 14 MoO_6 octahedra having different Mo−O bond distances are listed in Supporting Information Table S1. In comparison, the parent compound $SiMo_{12}$-bpy_3 does not show any tilting between the POMs cluster (Figure 2a). Figure 3 shows different orientation of 4,4′-bpy in the compounds $SiMo_{14}$-bpy_2 and $SiMo_{12}$-bpy_3. $SiMo_{14}$-bpy_2 has four different types of 4,4′-bpy orientations compared to two types in $SiMo_{12}$-bpy_3.

It is worthwhile also to compare the crystal structure of ($SiMo_{14}$-bpy_2) with the parent compound ($SiMo_{12}$-bpy_3). The asymmetric unit in the parent compound ($SiMo_{12}$-bpy_3) consists of half of an *α*-Keggin $[HSiMo_{12}O_{40}]^{3-}$ anion and one and a half monoprotonated independent 4,4′-bpy ligands. One way of seeing the orientation can be explained by marking two distinct layers as A and B in Figure 4a. Nitrogen of the 4,4′-bpy interacts with the oxygen of the POM in a linear fashion. In the case of ring A the N···O bond distance (shown in pink color) acts as a N−H−O bond with distances of 3.020(6) and 3.036(3) Å while the nitrogen at B has the N···O bond distances 3.010(5) and 3.011(5) Å. The dihedral angle of the two types are 4,4′-bpy rings 23.827(9)° and 43.954(7)°. On the other hand, the 4,4′-bpy rings in $SiMo_{14}$-bpy_2 interact with POMs in a nonlinear fashion with a tilting angle of 41.12(2)° in the $SiMo_{14}O_{44}$ unit and varying torsional angle of 41.69(1)° and 23.556(9)° in the 4,4′-bpy rings. The N···O distance (shown in pink color) between the POM and the 4,4′-bpy is in two different ranges: 2.58−2.83 and 3.12−3.30 Å. The hydrogen bonding of the C−H···O (shown in black color) between the 4,4′-bpy and the POM is in the range 2.32−2.61 Å. Both the layers are made up of one set of 4,4′-bpy which grows along the *ac* plane marked with black bonds while another is along the *bc* plane in the opposite direction marked in red bonds. This orientation difference is attributed to the tilting angle of the POM unit. It is interesting to note that the two 4,4′-bpy molecules are placed near the $\{MoO_2\}$ units of the POM. The 4,4′-bpy acts as bridging between two POMs units forming H-bonding between nitrogen of the 4,4′-bpy and oxygen of the $\{MoO_2\}$ unit with distances in the range 3.60−4.04 Å.

4.1. IR Spectroscopy. The infrared spectra measured in the region 1100−400 cm^{-1} for the compounds $SiMo_{14}$-bpy_2 and $SiMo_{12}$-bpy_3 are shown in Figure 5. The peaks at 1593(s), 1535(s), 1490(s), and 1416(m) cm^{-1} correspond to the aromatic C=C stretching while the peaks at 1221(s) and 1176(w) cm^{-1} correspond to Ar−H in-plane stretching and the peaks at 1043(m) and 995(s) cm^{-1} correspond to Ar−H out-of-plane stretching. The vibrational peak at 611 cm^{-1} is a very sensitive peak which is susceptible to coordination with the metal atom.[55] This peak is found to be very weak in both cases. The single crystal data suggests that there are very weak interactions of the POM with the nitrogen of the 4,4′-bpy with a distance of around 3.30 Å. The low wavenumber (~<1000 cm^{-1}) region in the IR spectra of both compounds corresponds to the characteristic peaks of the polyoxometalate. The

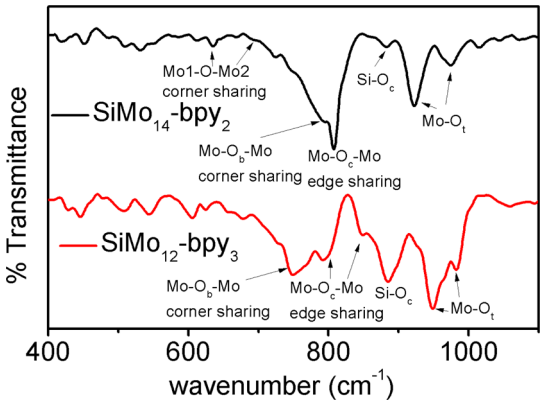

Figure 5. FT-IR spectra of both hybrid materials $SiMo_{14}$-bpy_2 and $SiMo_{12}$-bpy_3. The important stretching frequencies are marked with arrows.

compound $SiMo_{14}$-bpy_2 shows a more complex spectrum than the compound $SiMo_{12}$-bpy_3 especially in the region 1000−600 cm^{-1}. The strong peak observed at 940 cm^{-1} for the compound $SiMo_{12}$-bpy_3 corresponds to the (Mo−O_t) bond indicating only one type of terminal oxygen bond. However, these stretching vibrations become complex due to the introduction of the two capped $\{MoO_2\}$ units in the $SiMo_{14}$-bpy_2 structure. The crystal structure of $SiMo_{14}$-bpy_2 consists of three different terminal bond lengths: one from the Mo−O_t of the octahedral corresponding to the strong peak at 953 cm^{-1}, and the peaks at 983 and 971 cm^{-1} correspond to the terminal (Mo−O_t) of the $\{MoO_2\}$ unit, respectively. The effect and the presence of the $\{MoO_2\}$ unit in the crystal structure become more clear from the Mo−O_b−Mo corner sharing bonds. The broad peaks at 683 and 634 cm^{-1} correspond to the Mo−O_b−Mo stretching between Mo of $\{MoO_2\}$ unit and the adjacent Mo atom of the MoO_6 confirming the corner sharing of the $\{MoO_2\}$ unit.[56] This shift is due to the larger bond length of one of the bonds, 2.19 Å. The vibrational frequencies of the polyoxometalates $SiMo_{14}$-bpy_2 and $SiMo_{12}$-bpy_3 are compared in Table S2 in the Supporting Information.

4.2. UV−Vis Spectroscopy. The diffused reflectance spectrum (DRS) for the compounds $SiMo_{14}$-bpy_2 and $SiMo_{12}$-bpy_3 is shown in the Supporting Information (Figure S3). The DRS data was then converted to absorbance (Figure 6) using the Kubelka−Munk equation $F = \alpha/S = (1 - R)^2/2R$, where *R* is the reflectance of an infinitely thick layer at a given wavelength.[57] It is already known that 4,4′-bpy shows a

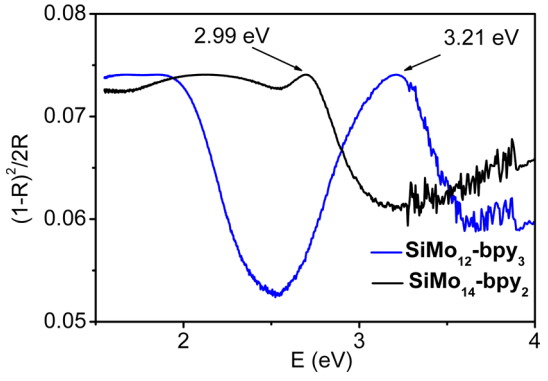

Figure 6. *K*−*M* function vs energy (eV) curve for the compounds $SiMo_{14}$-bpy_2 and $SiMo_{12}$-bpy_3.

dx.doi.org/10.1021/ic402858u | *Inorg. Chem.* 2014, 53, 653−660

predominant peak at 238 nm corresponding to the $\pi-\pi^*$ transition.[44] There was no visible shift observed in the case of $SiMo_{12}$-bpy_3 while a red shift is observed at 247 nm for $SiMo_{14}$-bpy_2, which is an indication for the weaker bonding between the POM and the 4,4′-bpy. The spectrum of 4,4′-bpy also has a broad peak in the region 320−375 nm (corresponding to the $n-\pi^*$ transition), which is shifted to 387 nm for $SiMo_{12}$-bpy_3 and 457 nm for $SiMo_{14}$-bpy_2. This red shift in the hybrid materials indicates that the 4,4′-bpy system has lost its rigidity within the system,[58] which is later confirmed from the fluorescence measurement.

The band gap (E_g) was determined as the intersection point between the energy axis and the line extrapolated from the linear portion of the absorption edge in a plot of the Kubelka−Munk function F against energy E.[59] The band gaps were found to be 2.99 eV for $SiMo_{14}$-bpy_2 and 3.21 eV for $SiMo_{12}$-bpy_3 indicating they are semiconductors. It is interesting to note that both 4,4′-bpy (4.23 eV) and POM $[SiMo_{12}O_{40}]^{4-}$ (4.73 eV) are insulators inherently.[60] The interaction between 4,4′-bpy with the POM probably affects energy levels near the Fermi level to make the hybrid as a good semiconductor.

4.2. Fluorescence Spectroscopy. The fluorescence spectroscopy was performed at 303 K for free 4,4′-bpy, $SiMo_{14}$-bpy_2, and $SiMo_{12}$-bpy_3 in the solid state (Figure 7). The 4,4′-bpy upon excitation at 358 nm gave 4 emission peaks at 483, 456, 445, and 420 nm. The samples $SiMo_{14}$-bpy_2 and $SiMo_{12}$-bpy_3 were excited at 326 nm, and all four emission peaks of 4,4′-bpy were observed: 483, 460, 468, and 420 nm for $SiMo_{14}$-bpy_2 and 483, 452, 435, and 420 nm for $SiMo_{12}$-bpy_3. The peaks at 460 and 468 nm in $SiMo_{14}$-bpy_2 are red-shifted in comparison with the free 4,4′-bpy peaks of 445 and 456 nm, indicating a weaker interaction of the polyoxometalate with the 4,4′-bpy rings in $SiMo_{14}$-bpy_2. The blue shift in this compound also can be attributed due to the rigidity in the 4,4′-bpy system and the loss of energy via radiationless decay of the intraligand emission in the excited state. This indicates that the new compound $SiMo_{14}$-bpy_2 is capable of producing blue light in electroluminescent devices.[58] The peaks at 452 and 435 nm for $SiMo_{12}$-bpy_3 are red-shifted compared to 4,4′-bpy suggesting a stronger interaction of the 4,4′-bpy with the POM which in fact resulted in the 3D structure of the compound.

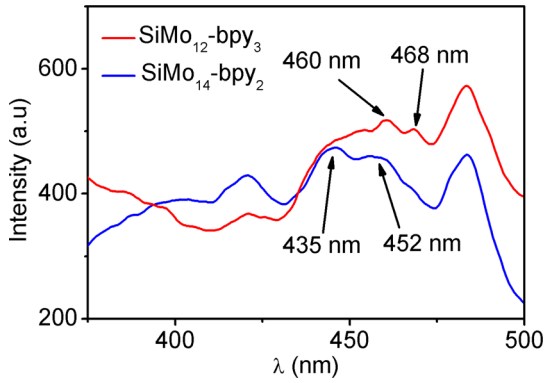

Figure 7. Fluorescence spectra of the compounds $SiMo_{14}$-bpy_2 and $SiMo_{12}$-bpy_3 excited at 326 nm.

4.3. Magnetic Measurement. Magnetic measurements of the compound $SiMo_{14}$-bpy_2 was performed on a powdered crystalline sample from 2 to 300 K at 1000 Oe. The temperature dependent molar magnetic susceptibility ($\chi_M T$) and inverse susceptibility (χ^{-1}) for the compound $SiMo_{14}$-bpy_2 are shown in Figure 8. The inset in Figure 8 shows a small hump at 18 K which is an indication of either weak antiferromagnetic ordering or spin reordering at this temperature. The inverse susceptibility curve above 70 K obeys the Curie−Weiss law $\chi(T) = C/(T - \theta_p)$ where C is Curie constant ($N_A\mu_{eff}^2/3K_bT$) and θ_p is the Weiss constant. A fit to the curve above 70 K resulted in an effective magnetic moment (μ) of 2.71 μ_B/ formula. The estimated magnetic moment suggests that there is a contribution of magnetic Mo^{+V} (1.723 μ_B) which is corroborating the crystal structure and XPS data suggesting the material contains Mo^{+V} and Mo^{+VI}. $SiMo_{12}$-bpy_3 is a weak magnetic material (Pauli paramagnet) compared to $SiMo_{14}$-bpy_2 as shown in Supporting Information Figure S4. The negative value of χ in emu mol at 303 K for $SiMo_{12}$-bpy_3 indicates the diamagnetic behavior and can rule out the presence of pentavalent Mo in the compound.

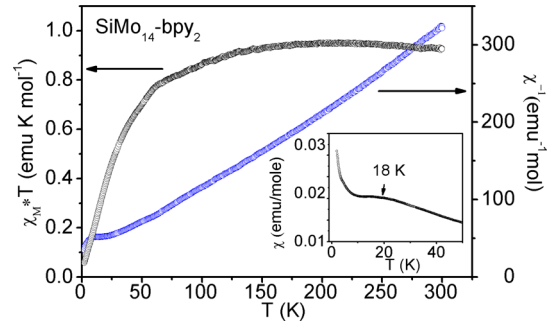

Figure 8. Magnetic susceptibility ($\chi_M T$) and inverse susceptibility for the sample $SiMo_{14}$-bpy_2 within the temperature range 2−300 K. The inset figure shows a hump at 18 K indicates either a probable weak antiferromagnetic ordering or spin reorientation.

4.4. X-ray Photoelectron Spectroscopy. The mixed valence state of Mo in the compound $SiMo_{14}$-bpy_2 was further confirmed by the XPS measurement. Figure 9 shows the XPS data of the compound $SiMo_{14}$-bpy_2 measured at room temperature, and further details are listed in Supporting Information Table S3. The 3d region of Mo was studied, and upon deconvolution four well resolved peaks were observed at 231.23 (4), 232.62 (1), 234.6 (2), and 235.72 (4) eV, attributed to Mo^{+V} $3d_{5/2}$, Mo^{+VI} $3d_{5/2}$, Mo^{+V} $3d_{3/2}$, and $Mo^{+VI}3d_{3/2}$,

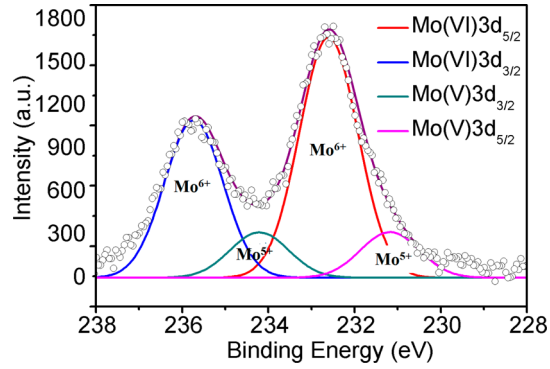

Figure 9. XPS spectra of $SiMo_{14}$-bpy_2 measured at 303 K. The open circle represents the raw data of the measurement. The violet solid curve is the fit by the Levenberg−Marquardt method. The fitting contains four different peaks: Mo (VI) $3d_{3/2}$ (blue), Mo (VI) $3d_{5/2}$ (green), Mo (V) $3d_{3/2}$ (green), and Mo (V) $3d_{5/2}$ (pink).

dx.doi.org/10.1021/ic402858u | Inorg. Chem. 2014, 53, 653−660

respectively.[61] The intensity ratio between Mo^{+V} and Mo^{+VI}, calculated using the formula $C = (I_x/S_x)/E(I_x/S_x)$ where I_x = intensity and S_x = sensitivity factor (2.867),[62] is 15:85, exactly corroborating with the BVS calculations as well as the magnetic data.

CONCLUSION

We have synthesized a new supramolecular inorganic−organic hybrid material constructed from polyoxometalates and 4,4′-bpyridine. This compound is unusually capped with $\{MoO_2\}$ unit on the α-Keggin structure and interacts with 4,4′-bpyridine rings through electrostatic and hydrogen bonding. A detailed comparison is made of this material with its parent compound $[(SiMo_{12}O_{40})\ (4,4'\text{-Hbpy})_3]$ using the single crystal X-ray diffraction data. The tilting and geometric strain of the 4,4′-bpyridine rings plays a crucial role in the architecture of this new structure. The valence band sum calculations showed that two Mo atoms in the capping unit are in the pentavalent state and the remaining Mo atoms are in the hexavalent state. This mixed valent Mo state is later observed in the magnetic measurement and quantitatively confirmed by XPS measurements. In addition to geometric strain, +5 oxidation state of Mo seems to play a significant role in the formation of the new compound which further affects the band structure with insulator to semiconductor transition from the parent components POMs and 4,4′-bpyridine. The orientation of the 4,4′-bipyridine was observed to play a significant role in the crystal packing. Further work in this area will be focused on the synthesis of other novel metal cluster aggregations by adopting appropriate reaction conditions and ligands.

ASSOCIATED CONTENT

Supporting Information

Crystallographic information file (CIF) for $SiMo_{14}$-bpy_2, table of bond lengths, and the coordination sphere of each MoO_6 octahedral unit of $SiMo_{14}$-bpy_2. Table of IR absorption frequencies for the compounds $SiMo_{14}$-bpy_2 and $SiMoO_{12}$-bpy_3, table of XPS binding energy of 3d orbitals for $SiMo_{14}$-bpy_2, EDAX spectrum, and temperature dependent magnetic susceptibility plots for $SiMo_{14}$-bpy_2 and $SiMoO_{12}$-bpy_3. This material is available free of charge via the Internet at http://pubs.acs.org.

AUTHOR INFORMATION

Corresponding Author

*E-mail: sebastiancp@jncasr.ac.in. Phone: 080-22082998. Fax: 080-22082627.

Notes

The authors declare no competing financial interest.

ACKNOWLEDGMENTS

We thank Professor C.N.R. Rao for his support and guidance. Financial support from the DST (Grant SR/S2/RJN-24/2010), Sheik Saqr Laboratory, and JNCASR is gratefully acknowledged. S.C.P. thanks DST for the Ramanujan Fellowship.

REFERENCES

(1) Lehn, J. M. *Supramolecular Chemistry*; VCH: New York, 1995.
(2) Rao, C. N. R.; Natarajan, S.; Vaidhyanathan, R. *Angew. Chem., Int. Ed.* **2004**, *43*, 1466.
(3) Yaghi, O. M.; O'Keeffe, M.; Ockwig, N. W.; Chae, H. K.; Eddaoudi, M.; Kim, J. *Nature* **2003**, *423*, 705.
(4) Rowsell, J. L. C.; Yaghi, O. M. *Microporous Mesoporous Mater.* **2004**, *73*, 3.
(5) Abrahams, B. F.; Hudson, T. A.; Robson, R. *J. Am. Chem. Soc.* **2004**, *126*, 8624.
(6) Ying, J.; Min-Hou; Liu, X. J.; Tian, A. X.; Wang, X. L. *J. Coord. Chem.* **2012**, *65*, 218.
(7) Hagrman, P. J.; Hagrman, D.; Zubieta, J. *Angew. Chem., Int. Ed.* **1999**, *38*, 2639.
(8) Cheetham, A. K.; Ferey, G.; Loiseau, T. *Angew. Chem., Int. Ed.* **1999**, *38*, 3268.
(9) Ferey, G. *Chem. Mater.* **2001**, *13*, 3084.
(10) Cardona-Serra, S.; Clemente-Juan, J. M.; Coronado, E.; Gaita-Arino, A.; Camon, A.; Evangelisti, M.; Luis, F.; Martinez-Perez, M. J.; Sese, J. *J. Am. Chem. Soc.* **2012**, *134*, 14982.
(11) Ritchie, C.; Ferguson, A.; Nojiri, H.; Miras, H. N.; Song, Y. F.; Long, D. L.; Burkholder, E.; Murrie, M.; Kogerler, P.; Brechin, E. K.; Cronin, L. *Angew. Chem., Int. Ed.* **2008**, *47*, 5609.
(12) Zhang, Z. M.; Yao, S.; Li, Y. G.; Wu, H. H.; Wang, Y. H.; Rouzieres, M.; Clerac, R.; Su, Z. M.; Wang, E. B. *Chem. Commun.* **2013**, *49*, 2515.
(13) Austria, C.; Zhang, J.; Valle, H.; Zhang, Q.; Chew, E.; Nguyen, D. T.; Gu, J. Y.; Feng, P.; Bu, X. *Inorg. Chem.* **2007**, *46*, 6283.
(14) Zheng, S. T.; Chen, Y. M.; Zhang, J.; Xu, J. Q.; Yang, G. Y. *Eur. J. Inorg. Chem.* **2006**, 397.
(15) Lu, Y.; Xu, Y.; Wang, E. B.; Lu, J.; Hu, C. W.; Xu, L. *Cryst. Growth Des.* **2005**, *5*, 257.
(16) Dolbecq, A.; Mellot-Draznieks, C.; Mialane, P.; Marrot, R.; Ferey, G.; Secheresse, F. *Eur. J. Inorg. Chem.* **2005**, 3009.
(17) Soumahoro, T.; Burkholder, E.; Ouellette, W.; Zubieta, J. *Inorg. Chim. Acta* **2005**, *358*, 606.
(18) Cui, X. B.; Xu, J. Q.; Sun, Y. H.; Li, Y.; Ye, L.; Yang, G. Y. *Inorg. Chem. Commun.* **2004**, *7*, 58.
(19) Jin, H.; Qi, Y. F.; Wang, E. B.; Li, Y. G.; Wang, X. L.; Qin, C.; Chang, S. *Cryst. Growth Des.* **2006**, *6*, 2693.
(20) Shi, Z. Y.; Gu, X. J.; Peng, J.; Yu, X.; Wang, E. B. *Eur. J. Inorg. Chem.* **2006**, 385.
(21) An, H. Y.; Wang, E. B.; Xiao, D. R.; Li, Y. G.; Su, Z. M.; Xu, L. *Angew. Chem., Int. Ed.* **2006**, *45*, 904.
(22) Lu, J.; Shen, E. H.; Yuan, M.; Li, Y. G.; Wang, E. B.; Hu, C. W.; Xu, L.; Peng, J. *Inorg. Chem.* **2003**, *42*, 6956.
(23) Liu, S. X.; Xie, L. H.; Gao, B.; Zhang, C. D.; Sun, C. Y.; Li, D. H.; Su, Z. M. *Chem. Commun.* **2005**, 5023.
(24) Dolbecq, A.; Mialane, P.; Lisnard, L.; Marrot, J.; Secheresse, F. *Chem.—Eur. J.* **2003**, *9*, 2914.
(25) Lu, J. J.; Xu, Y.; Goh, N. K.; Chia, L. S. *Chem. Commun.* **1998**, 2733.
(26) Liu, C. M.; Zhang, D. Q.; Xiong, M.; Zhu, D. B. *Chem. Commun.* **2002**, 1416.
(27) Tripathi, A.; Hughbanks, T.; Clearfield, A. *J. Am. Chem. Soc.* **2003**, *125*, 10528.
(28) Gao, J. K.; Cao, S. W.; Tay, Q. L.; Liu, Y.; Yu, L. M.; Ye, K. Q.; Mun, P. C. S.; Li, Y. X.; Rakesh, G.; Loo, S. C. J.; Chen, Z.; Zhao, Y.; Xue, C.; Zhang, Q. C. *Sci. Rep.* **2013**, 3.
(29) Gao, J. K.; Liu, X. F.; Liu, Y.; Yu, L. L.; Feng, Y. H.; Chen, H. Y.; Li, Y. X.; Rakesh, G.; Huan, C. H. A.; Sum, T. C.; Zhao, Y.; Zhang, Q. C. *Dalton Trans.* **2012**, *41*, 12185.
(30) Liu, Y.; Yu, L. M.; Loo, S. C. J.; Blair, R. G.; Zhang, Q. C. *J. Solid State Chem.* **2012**, *191*, 283.
(31) Zhang, Q. C.; Bu, X. H.; Lin, Z.; Wu, T.; Feng, P. Y. *Inorg. Chem.* **2008**, *47*, 9724.
(32) Zhang, Q. C.; Wu, T.; Bu, X. H.; Tran, T.; Feng, P. Y. *Chem. Mater.* **2008**, *20*, 4170.
(33) Kolotuchin, S. V.; Fenlon, E. E.; Wilson, S. R.; Loweth, C. J.; Zimmerman, S. C. *Angew. Chem., Int. Ed.* **1995**, *34*, 2654.
(34) Sanchez, C.; Soler-Illia, G. J. D. A.; Ribot, F.; Lalot, T.; Mayer, C. R.; Cabuil, V. *Chem. Mater.* **2001**, *13*, 3061.
(35) Song, Y. F.; Tsunashima, R. *Chem. Soc. Rev.* **2012**, *41*, 7384.
(36) Biradha, K.; Sarkar, M.; Rajput, L. *Chem. Commun.* **2006**, 4169.
(37) Biradha, K.; Sarkar, M.; Rajput, L. *Chem. Commun.* **2006**, 4169.

(38) Jeong, S.; Kim, D.; Song, X.; Choi, M.; Park, N.; Lah, M. S. *Chem. Mater.* **2013**, *25*, 1047.
(39) Maji, T. K.; Kitagawa, S. *Pure Appl. Chem.* **2007**, *79*, 2155.
(40) Song, J. L.; Zhao, H. H.; Mao, J. G.; Dunbar, K. R. *Chem. Mater.* **2004**, *16*, 1884.
(41) Wang, H. N.; Meng, X.; Qin, C.; Wang, X. L.; Yang, G. S.; Su, Z. M. *Dalton Trans.* **2012**, *41*, 1047.
(42) Xiao, L. N.; Wang, Y.; Peng, Y.; Li, G. H.; Xu, J. N.; Wang, L. M.; Hu, Y. Y.; Wang, T. G.; Gao, Z. M.; Zheng, D. F.; Cui, X. B.; Xu, J. Q. *Inorg. Chim. Acta* **2012**, *387*, 204.
(43) Liu, Y. B.; Wang, Y.; Xiao, L. N.; Hu, Y. Y.; Wang, L. M.; Cui, X. B.; Xu, J. Q. *J. Coord. Chem.* **2012**, *65*, 4342.
(44) Yang, H. X.; Lin, X.; Xu, B.; You, Y.; Cao, M. N.; Gao, S. Y.; Cao, R. *J. Mol. Struct.* **2010**, *966*, 33.
(45) Ma, F. X.; Zhao, Q. *Acta Crystallogr., Sect. E* **2008**, *64*, M1224.
(46) Dolbecq, A.; Cadot, E.; Eisner, D.; Secheresse, F. *Inorg. Chem.* **1999**, *38*, 4217.
(47) Wei, P. H.; Yuan, D.; Zhu, W. C.; Zhang, X. T.; Hu, B. *Acta Crystallogr., Sect. E* **2010**, *66*, M190.
(48) *SAINT 6.02 ed.*; Bruker AXS: Madison, WI, 1999.
(49) Sheldrick, G. M. University of Göttingen: Göttingen, Germany, 1997.
(50) Sheldrick, G. M.; Schneider, T. R. *Macromol. Crystallogr. B* **1997**, *277*, 319.
(51) Farrugia, L. J. *J. Appl. Crystallogr.* **1999**, 32.
(52) Pope, M. T.; Muller, A. *Angew. Chem., Int. Ed.* **1991**, *30*, 34.
(53) Haushalter, R. C.; Mundi, L. A. *Chem. Mater.* **1992**, *4*, 31.
(54) Brese, N. E.; Okeeffe, M. *Acta Crystallogr., Sect. B* **1991**, *47*, 192.
(55) Podgajny, R.; Balanda, M.; Sikora, M.; Borowiec, M.; Spalek, L.; Kapusta, C.; Sieklucka, B. *Dalton Trans.* **2006**, 2801.
(56) Thouvenot, R.; Fournier, M.; Raymonde, F.; Rocchiccioli-Deltcheff, C. *Inorg. Chem.* **1984**, *23*, 598.
(57) Kortun, G. *Reflectance Spectroscopy*; Springer-Verlag: New York, 1969.
(58) Song, J. L.; Zhao, H. H.; Mao, J. G.; Dunbar, K. R. *Chem. Mater.* **2004**, *16*, 1884.
(59) Pankove, J. I. *Optical Processes in Semiconductors*; Prentice-Hall: Englewood Cliffs, NJ, 1971.
(60) Stokes, E. B. *State-of-the-Art Program on Compound Semiconductors XXXVIII and Wide Bandgap Semiconductors for Photonic and Electronic Devices and Sensors III: Proceedings of the International Symposia*; Electronics Division and Sensor Divison, Electrochemical Society, 2003.
(61) Choi, J. G.; Thompson, L. T. *Appl. Surf. Sci.* **1996**, *93*, 143.
(62) Wagner, C. D.; Riggs, W. M.; Davis, L. E.; Moulder, J. F.; Muilenberg, G. E. *Handbook of X-ray Photoelectron Spectroscopy*; Perkin-Elmer Corp., Physical Electronics Division: Eden Prairie, Minnesota, 1979.